analytical chemistry

pubs.acs.org/ac Article

Ultrasensitive Photoelectrochemical Biosensor for microRNA-155 Based on Energy Transfer between Au Nanocages and Red Emission Carbon Dot-Assembled Nanosheets Coupled with the Duplex-Specific Nuclease Enzyme-Assisted Target Recycling Strategy

Jiao Yang, Fang Luo, Jian Wang, Bin Qiu, Jie Shen,* Lin Zhang,* and Zhenyu Lin*

Cite This: *Anal. Chem.* 2022, 94, 1482−1490 Read Online

ACCESS | Metrics & More | Article Recommendations | Supporting Information

ABSTRACT: Energy transfer (ET) is an effective tool to construct photoelectrochemical (PEC) biosensors for its high sensitivity. Since the materials to develop ET systems are limited, exploring new and universal ET systems is significant. Herein, new photoactive nanosheets (R-CDs NS) formed by self-assembling of red emission carbon dots (R-CDs) have been synthesized, which exhibit wide visible light absorption and stable photocurrent response and have an obvious sensitization effect for TiO_2. Gold nanocages (AuNCs), whose absorption overlap well with the R-CDs' emission, were synthesized and served as PEC quenchers for the photosensitized system that consists of TiO_2 and R-CDs. The ET between R-CDs and AuNCs can boost the recombination of photogenerated electron−hole pairs of R-CDs and results in a quenched photocurrent of this system. MicroRNA-155 was chosen as a model target. First, the nanocomposite containing R-CDs NS and AuNCs was prepared through DNA modification and hybridization. In the absence of the target, AuNCs and R-CDs were close enough for ET, with TiO_2-modified FTO serving as the working electrode, and a quenched photocurrent was detected. In the presence of the target, the disintegration of the nanocomposite was induced through target hybridization and DNA hydrolyzation, leading to the separation of AuNCs and R-CDs NS, and the ET disappeared and led to a high photocurrent. With duplex-specific nuclease enzyme-assisted target recycling, the high sensitivity enabled the sensor to monitor the target in cancer cells. The sensor has a low detection limit of 71 aM. The sensing platform has high sensitivity, good selectivity, and reproducibility.

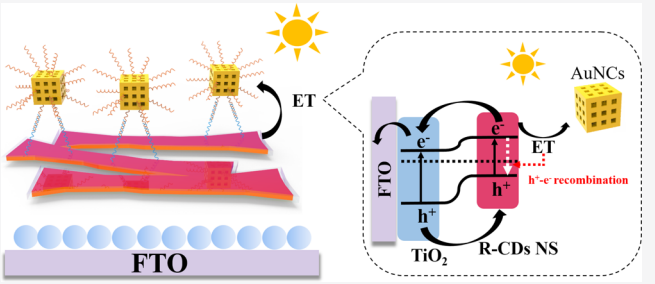

INTRODUCTION

Photoelectrochemical (PEC) biosensing is an elegant methodology, which has been widely used in detection of diverse biomarkers.[1−5] Since the quenching effect of gold nanoparticles (AuNPs) to the PEC response of CdS quantum dots (QDs) through an energy transfer (ET) process that had been reported in 2011, ET become an effective mean in the development of PEC biosenors.[6−9] The strong ET in general needs close proximity and sufficient overlap between the emission of quantum dots (energy donor) and the plasmon band of noble metal nanoparticles (energy acceptor), which can promote the recombination of photogenerated electron−hole pairs of the energy donor and reduce the photocurrent response.[10] However, due to the surface plasmon resonance (SPR) absorption of the frequently used spherical AuNPs centered at 520 nm, the photoactive materials, which can be coupled with AuNPs, are limited, and the mostly used one is CdS QDs (emission centered at 510 nm), which have a negative impact on human beings and the environment. It is of great significance to explore environment-friendly and universal nanomaterials to construct new ET systems.

Carbon dots (CDs) have the advantages of biocompatibility, non-toxicity, and low environmental impact, making them an alternative to traditional CdS quantum dots.[11] Blue emission CDs with visible light absorption and a narrow band gap have been used as photosensitizers for TiO_2 to construct PEC biosensors.[12,13] Recently, red emission carbon dots (R-CDs) have aroused wide concern because of their high resistance to photobleaching, and more importantly, R-CDs have stronger absorption in the visible light region and a narrower band gap than conventional blue or green emission CDs,[14−19] which make contributions to the improved light absorption and enhanced PEC response of TiO_2. However, R-CDs often have a higher dehydration and carbonization degree, and thus, most R-CDs exhibit poor hydrophilicity and their biosensing

Received: November 23, 2021
Accepted: December 22, 2021
Published: December 30, 2021

https://doi.org/10.1021/acs.analchem.1c05081
Anal. Chem. 2022, 94, 1482−1490

application is limited.[18] It has been found that when the solvent of prepared R-CDs changed from ethanol to deionized water, the R-CDs will self-assemble to form thin nanosheets (named R-CDs NS) due to the hydrophobic interaction. The obtained R-CDs NS not only exhibits wide absorption but also has a stable PEC response and also has an obvious sensitization effect for TiO_2, which makes the obtained R-CDs NS become a promising candidate for new photoactive nanomaterials.

To establish an ET-based PEC biosensor, noble metal nanoparticles, which have strong absorption in the NIR region and overlap as much as possible with the emission of R-CDs, are needed. Au nanocages (AuNCs), with a hollow and porous nanostructure, have been widely used as photothermal agents and drug delivery vehicles due to their unique structure and strong absorption in the NIR region.[20−24] Compared to the commonly used spherical AuNPs whose SPR absorption centered at 520 nm, the SPR peak of AuNCs can be precisely tuned to any wavelength in the NIR region by controlling their size or wall thickness.[25] Moreover, the surface modification of AuNCs based on Au−S bonds can be easily realized through a robust and straightforward procedure, which makes AuNCs an excellent candidate for energy acceptor of R-CDs NS, and a new ET system can be established.

In this study, an R-CDs NS and AuNC-based ET system were utilized to develop a PEC biosensor for the first time. MicroRNA-155 (miRNA-155) has been chosen as a model target, which is a biomarker for multiple cancers.[26−28] First, the nanocomposite containing R-CDs NS and AuNCs was prepared through DNA modification and hybridization, and AuNCs and R-CDs were close enough for ET, with TiO_2-modified FTO serving as a working electrode, the photocurrent of the photosensitized system consists of TiO_2 and R-CDs that was quenched by AuNCs through ET between R-CDs and AuNCs. In the presence of the target, the disintegration of the nanocomposite was induced by the target through DNA hybridization and hydrolyzation, leading to the separation of AuNCs and R-CDs NS. Since the ET was distance-dependent, ET cannot happen and a high photocurrent of the system can be detected. With a duplex-specific nuclease (DSN) enzyme-assisted target recycling amplification strategy, the proposed PEC senor had a high sensitivity, good selectivity, and reproducibility.

EXPERIMENTAL SECTION

Reagents and Apparatus. The details of reagents and apparatus are shown in the Supporting Information.

Synthesis of Ag Nanocubes (AgNCs). The synthesis process was according to a previous study.[29] To prepare Au nanocages (AuNCs), Ag nanocubes served as a sacrificial template should be synthesized first. One hundred milliliters of ethylene glycol was added into a round-bottom flask and heated to 150 °C under magnetic stirring. Then, 0.36 mL of 3.0 mM NaSH in ethylene glycol was added under magnetic stirring. After 2 min, 3.0 mL of 3.0 mM HCl in ethylene glycol and 7.5 mL of 20 mg/mL PVP in ethylene glycol were added. After another 2 min, 2.4 mL of 282 mM CF_3COOAg in ethylene glycol was added and kept at 150 °C for 45 min. Finally, the flask was transferred from an oil bath to an ice bath to stop the reaction. Then, the solution was transferred to centrifuge tubes and twice the volume of acetone was added; after centrifuging at 4000 rpm for 20 min, the sediment was collected and resuspended in deionized water; then, the solution was centrifuged at 10,000 rpm and washed with anhydrous ethanol and deionized water two times, respectively; the collected product was resuspended in 15 mL of deionized water and stored at 4 °C in the dark before use.

Synthesis of AuNCs. Porous Au nanocages were obtained by Ag nanocubes through the galvanic replacement reaction.[25] Briefly, 5.0 mL of 1.0 mg/mL PVP and 100 μL of prepared Ag nanocubes were added into a round-bottom flask and heated to 90 °C. Then, 0.10 mM $HAuCl_4$ solution was added dropwise until the color of the solution turned to blue and kept at 90 °C for 10 min under magnetic stirring. Afterward, the solution was cooled to room temperature and transferred to centrifuge tubes, and NaCl powder was added until the solution was saturated, centrifuged at 8000 rpm for 10 min, and washed with deionized water three times, and the product was resuspended in 5.0 mL of deionized water and stored at 4 °C before use.

Synthesis of R-CD-Assembled Nanosheets. First, R-CDs were synthesized according to a previous study[15] with some modifications. Then, 306.67 mg of dopamine and 180.0 mg of 1,2-diaminobenzene were dissolved in 16.67 mL of deionized water, and the pH value was adjusted by adding 500 μL of HCl (36−38%). The obtained solution was transferred to a poly(tetrafluoroethylene) (Teflon)-lined autoclave (50 mL) and heated at 200 °C for 8 h. The reactor was cooled to room temperature, and the obtained solution was removed; then, the reactor was soaked by 15 mL of ethanol overnight, and the R-CDs in ethanol were obtained. Then, the solution of R-CDs was purified by a dialysis bag (with molecular weight cutoff: ∼3 kDa) in deionized water for 12 h, the deionized water was replaced every 3 h, and the R-CDs NS was obtained through self-assembling of R-CDs.

Synthesis of the R-CDs NS/HA/dsDNA/AuNCs Composite. To improve the hydrophilicity of R-CDs NS, hyaluronic acid (HA), a natural polymer material, which has good hydrophilicity due to its abundant carboxyl groups, was introduced. HA was modified on the surface of R-CDs NS via the connection of carboxyl groups and the amino groups. The synthesis process of the composite includes two parts: (i) synthesis of ssDNA-1/HA/R-CDs nanosheets: 200 μL of R-CDs nanosheet solution was mixed with 25 μL of 4.0 mg/mL HA, 10 μL of 97.6 mg/mL EDC, and 10 μL of 48 mg/mL NHS, and then, 100 μL of NEBuffer 2 and 10 μL of 100 μM ssDNA-1 were added, and the solution was incubated at 37 °C for 1 h. (ii) Synthesis of ssDNA-2-modified AuNCs: 5.0 μL of 1% Tween 20, 30 μL of 4.0 μM mPEG-SH, 5.0 μL of 100 μM ssDNA-2, and 10 μL of 3.0 M NaCl were added into 600 μL of AuNC solution and kept in the dark at room temperature for 1 h. After centrifugation at 8500 rpm for 10 min and washing with deionized water two times, ssDNA-2-modified AuNCs were resuspended in 1× NEBuffer 2 and kept at 4 °C before use. Afterward, the obtained solutions of (i) and (ii) were mixed and incubated at 37 °C for 2 h. Then, the solution was centrifuged at 6000 rpm for 10 min and washed twice with deionized water, and the R-CDs NS/HA/dsDNA/AuNCs composite was resuspended in 600 μL of 1× NEBuffer 2 and stored at 4 °C before use.

Procedures for MicroRNA Detection. First, the FTO electrode was washed by ethanol, acetone, and DI water. After the electrode was dried in the air, 10 μL of 1.0 mg/mL TiO_2 solution was dropped on the electrode in a valid area of 0.3 cm^2 and dried in the air. The TiO_2-modified FTO electrodes were calcined at 450 °C for 30 min. Second, 100 μL of R-CDs NS/HA/dsDNA/AuNCs composite mixed with 20 μL of

https://doi.org/10.1021/acs.analchem.1c05081
Anal. Chem. 2022, 94, 1482−1490

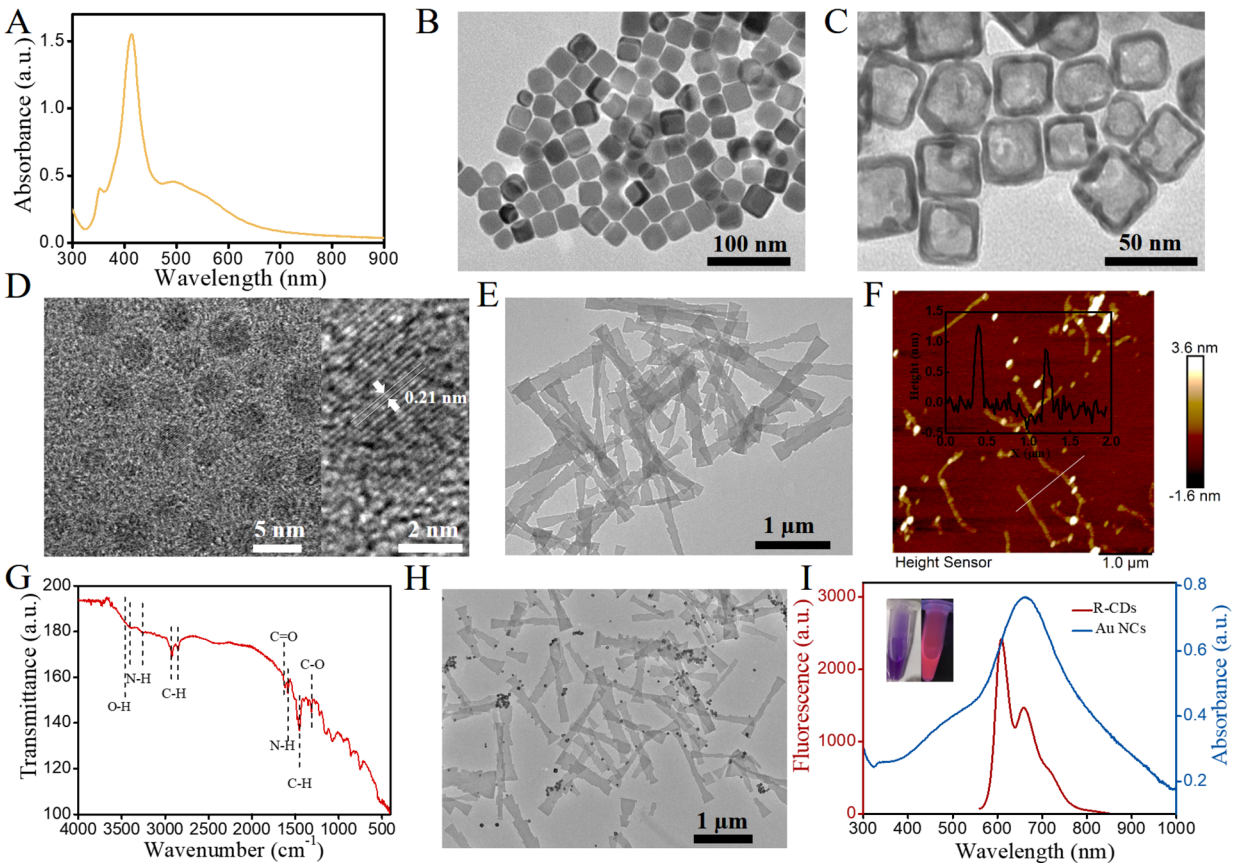

Figure 1. (A) UV−vis absorption spectrum and (B) TEM image of AgNCs. (C) TEM image of AuNCs. (D) TEM image of R-CDs; inset picture: HTEM image of R-CDs. (E) TEM image, (F) AFM image, and (G) FTIR spectrum of R-CDs NS. (H) TEM image of the R-CDs NS/HA/dsDNA/AuNCs composite. (I) FL emission spectrum of R-CDs in ethanol (red curve) at an optimal excitation wavelength of 542 nm (PMT voltage: 700 V, the slit widths: 5.0 nm) and UV−vis absorption spectrum of Au NCs (blue curve).

samples containing 0.10 U DSN and the target with different concentrations, the mixed solution was incubated at 37 °C for 1 h, and then 10 μL of stop buffer (10 mM EDTA, which can inhibit enzyme activity by chelating Mg^{2+} in buffer solution that DNS needs to maintain enzyme activity) was added to inactivate the DSN and stop the reaction. Finally, the obtained solution was added into a small quartz cell (with a small base area of 1.54 cm^2 to ensure the immersion of the three-electrode system by a small volume of sample) containing 200 μL of 10 mM PBS buffer, and the TiO_2-modified FTO electrode was immersed in the solution for PEC measurements.

RESULTS AND DISCUSSION

Characterization of Prepared Nanomaterials. As illustrated in Figure 1A, the UV−visible absorption spectrum of AgNCs exhibits its characteristic absorption peak of about 410 nm. Figure 1B shows the uniform morphology of AgNCs with a size of approximately 35 nm in an edge length. As illustrated in Figure 1C, the hollow and porous nanostructure of AuNCs with an average size of 35 nm can be observed clearly. Figure 1D shows TEM images of R-CDs, and the prepared R-CDs exhibit a uniform size of 5−8 nm. The high-resolution TEM image of R-CDs showed a typical lattice fringe with a distance of 0.21 nm. Figure 1E shows the TEM image of the raw R-CDs NS, which was in the shape of long strips, with a length of 1.0−1.5 μm and a width of 200− 300 nm. Also, Figure 1F illustrates the AFM image of the pure R-CDs NS, the thickness of the nanosheets was about 1.2 nm, and the morphology was consistent with Figure 1D. Figure 1G shows the FTIR spectrum of R-CDs NS, the peak at 1580 cm^{-1} corresponds to the bending vibration of N−H, and the peaks at 3405 and 3405 cm^{-1} correspond to the stretching vibration of N−H, which proved the abundant amino groups on the surface of R-CDs NS. Figure 1H displays the TEM image of the R-CDs NS/HA/dsDNA/AuNCs composite, and it can be clearly observed that the AuNCs were attached to the surface of R-CDs nanosheets due to the hybridization of ssDNA-1 and ssDNA-2. These results indicated the successful preparations of the nanomaterials. Figure 1I displays the broad SPR band (from 600 to 900 nm) centered at 658 nm of AuNCs in water (blue curve) and the FL emission spectrum centered at 650 nm of R-CDs in ethanol (red curve), and the inset pictures are the images of R-CDs in ethanol under sunlight (left) and a UV lamp (right, λ = 365 nm), respectively. The sufficient overlap between the emission of R-CDs and the plasmon band of AuNCs makes ET possible.

Principle of the ET-Based PEC Biosensor. As displayed in Scheme 1A, to improve the hydrophilicity of R-CDs NS and make the R-CDs NS stably dispersed in water, HA, which is rich in carboxyl groups, was introduced, and a large number of carboxyl groups of HA can connect with the amino groups of R-CDs NS with the help of EDC/NHS to form HA/R-CDs NS. Then, ssDNA-1 modified with amino groups can connect with HA/R-CDs NS to form ssDNA-1/HA/R-CDs NS. AuNCs can connect with ssDNA-2 through Au−S bonds to

https://doi.org/10.1021/acs.analchem.1c05081
Anal. Chem. 2022, 94, 1482−1490

Scheme 1. (A) Diagram of the Preparation of the R-CDs NS/HA/dsDNA/AuNCs Composite and (B) Principle of the ET-Based PEC Sensing Platform

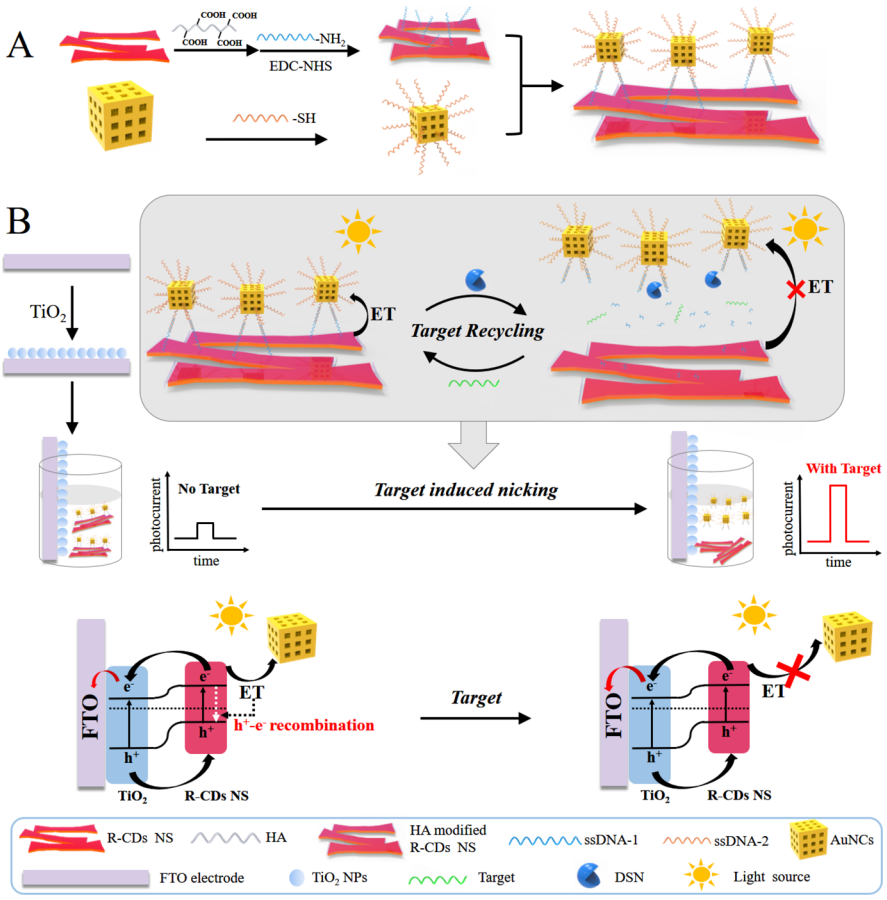

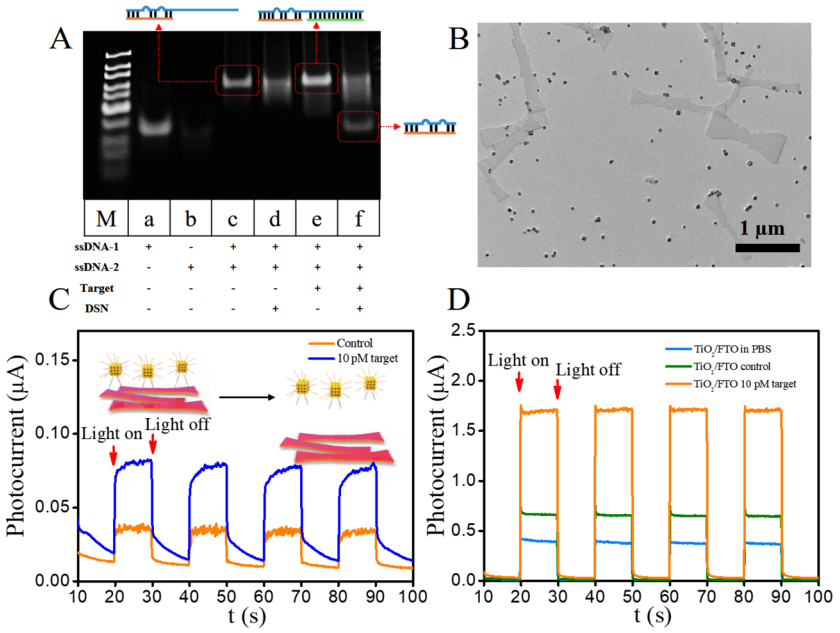

Figure 2. (A) Gel electrophoresis image of 5.0 μM ssDNA-1 (lane a), 5.0 μM ssDNA-2 (lane b, invisible due to its small molecular weight), 5.0 μM ssDNA-1 + ssDNA-2 (lane c), 5.0 μM ssDNA-1 + ssDNA-2 + target (lane d), 5.0 μM ssDNA-1 + ssDNA-2 + 0.1 U DSN (lane e), and 5.0 μM ssDNA-1 + ssDNA-2 + 2.0 μM target +0.1 U DSN (lane f). (B) TEM image of the R-CDs NS/HA/dsDNA/AuNCs composite after incubation with the target and DSN. Feasibility tests for different samples by using (C) clean FTO electrodes and (D) TiO_2-modified FTO electrodes.

form ssDNA-2/AuNCs. Afterward, the connection of ssDNA-2/AuNCs and ssDNA-1/HA/R-CDs NS was realized by the hybridization of ssDNA-1 and ssDNA-2 to form the R-CDs NS/HA/dsDNA/AuNCs composite. The principle of the

https://doi.org/10.1021/acs.analchem.1c05081
Anal. Chem. 2022, 94, 1482−1490

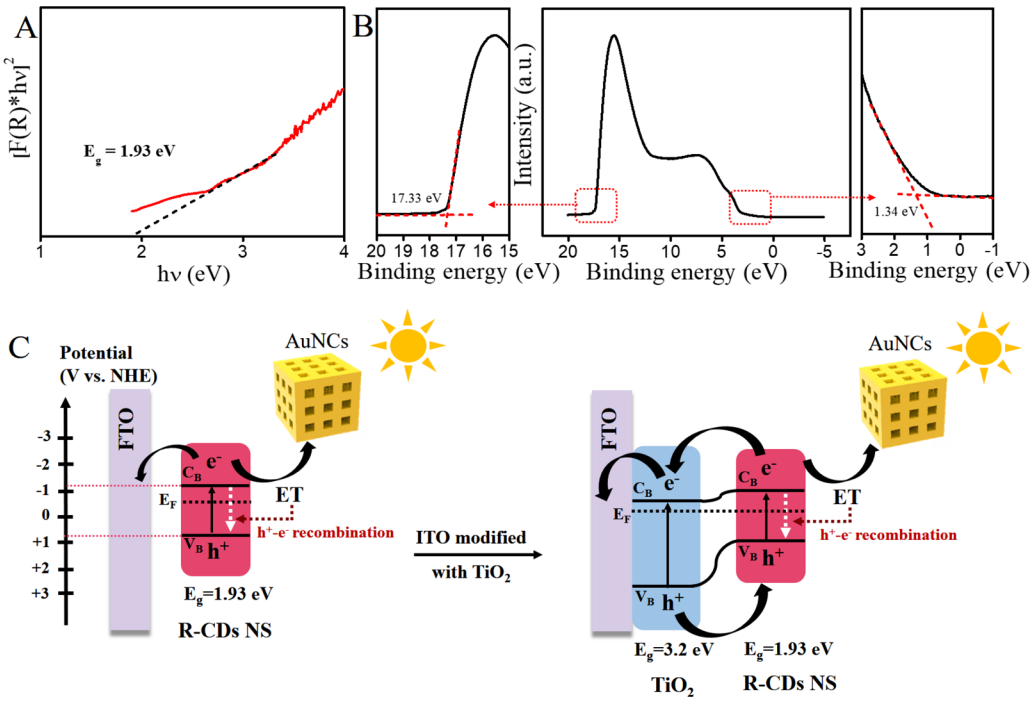

Figure 3. (A) UV−vis diffuse reflectance spectrum of R-CDs NS. (B) UPS survey spectrum of R-CDs NS. (C) Band alignment diagrams before and after the introduction of TiO_2.

proposed ET-based PEC sensor is shown in Scheme 1B, ssDNA-1 had two functional regions, one part was complementary with ssDNA-2, and another part was complementary with the target. The complementary part with ssDNA-2 was less than 10 bases and contains two-base mismatched sites, which cannot be nicked by DSN. Therefore, in the absence of the target, since the hybridized product of ssDNA-1 and ssDNA-2 (dsDNA) cannot be nicked by DSN, the AuNCs and R-CDs NS were close enough, and there was an effective ET process between R-CDs NS and AuNCs, which promoted the recombination of photogenerated electron−hole pairs of R-CDs NS; thus, a quenched photocurrent of the photosensitized system consists of TiO_2 and R-CDs can be detected. When the target was added into the solution of the R-CDs NS/HA/dsDNA/AuNCs composite, the target can hybridize with the single-strand part of dsDNA, which can bring about the nicking of ssDNA-1 with the help of DSN, the target was released to hybridize with another ssDNA-1 and induced another nicking and caused the separation of AuNCs and R-CDs NS, the far distance of AuNCs and R-CDs NS prevented the energy transfer process, and a high photocurrent of the system can be detected. The photocurrent enhanced gradually with the increase in the target concentration. Based on this, a sensitive PEC biosensor for the target can be developed. The mechanism of the photocurrent change before and after adding the target is also displayed in Scheme 1B; when the ET happened, the ET enhanced the recombination of photogenerated electron−hole pairs of R-CDs NS, and less electrons transferred to TiO_2, which caused less electrons flowing to the FTO electrode to generate a photocurrent, leading to a low photocurrent. On the contrary, when the ET cannot happen, more photogenerated electrons of R-CDs transferred to TiO_2 and more electrons flowed to the FTO electrode to generate a photocurrent, and a high photocurrent can be detected.

Feasibility Study. To validate the DSN enzyme-assisted target recycling, a polyacrylamide gel electrophoresis (PAGE) experiment was performed. As revealed in Figure 2A, lane c showed the bands of the hybridized product of ssDNA-1 and ssDNA-2. After adding DSN, the band position in lane d was almost the same with lane c, which proved that the hybridized product of ssDNA-1 and ssDNA-2 was not nicked by DSN. Lane e showed a bright band of the hybridized product of ssDNA-1, ssDNA-2, and the target. After adding DSN, a new band of nicking product in a smaller molecular weight can be observed in lane f, indicating that the hybridized product of ssDNA-1, ssDNA-2, and the target was nicked in the presence of the target, which proved the feasibility of the DSN enzyme-based amplification strategy. To figure out the change of the R-CDs NS/HA/dsDNA/AuNCs composite after the incubation with the target and DSN, the TEM characterization was carried out, as shown in Figure 2B, and many AuNCs separated from the surface of R-CDs NS, which proved the target induced nicking and the disintegration of the nanocomposite.

To demonstrate the feasibility of the ET-based PEC biosensor for miRNA-155 detection, a control assay was carried out, and the control group (no target) and experimental group (in the presence of the 1.0 pM target) were incubated with the prepared R-CDs NS/HA/dsDNA/AuNCs composite and DSN, respectively, and the resultant solution was collected for PEC tests. First, clean FTO electrodes were used for PEC tests, and the results are illustrated in Figure 2C; the photocurrent intensity of the experimental group was 1.1 times higher than that of the control, but the photocurrent intensity was relatively low. In order to improve the photocurrent intensity, TiO_2-modified electrodes were prepared and utilized for PEC tests, the results are displayed in Figure 2D, and it can be seen that the photocurrent intensity of the experimental group improved 18.9 times than that of clean FTO; meanwhile, the photocurrent intensity of the experimental group was 1.7

https://doi.org/10.1021/acs.analchem.1c05081
Anal. Chem. 2022, 94, 1482−1490

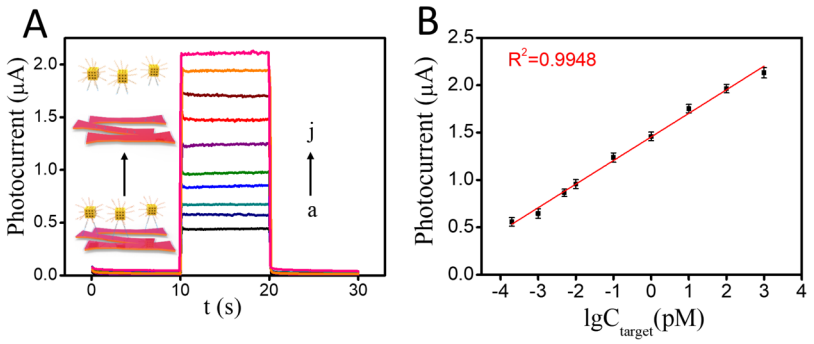

Figure 4. (A) PEC response with the increasing target concentration: (a–j) 0, 0.20 fM, 1.0 fM, 5.0 fM, 10 fM, 100 fM, 1.0 pM, 10 pM, 100 pM, and 1.0 nM. (B) Linear relationship between the photocurrent intensity and the logarithmic concentration of miRNA-155.

times higher than that of the control, which improved the sensitivity of the biosensor. Notably, the photocurrents of the control and experimental group were higher than the photocurrent when TiO_2-modified FTO was immersed in PBS buffer solution, which proved the sensitization effect of R-CDs to TiO_2.

Possible Mechanism of the Photocurrent Decrease by AuNCs and Enhancement on TiO_2-Modified Electrode by R-CDs NS. There are mainly two complex energy transfer paths between photoactive substances (energy donors) and precious metal nanoparticles (energy acceptors) in ET-based PEC systems, namely, exciton energy transfer (EET) and plasma resonance energy transfer (PRET).[6,30] EET means that the energy donor transfers energy to the acceptor in a non-radiation way, and the photogenerated electrons return to the ground state to recombine with holes. PRET means that the emission of energy donor triggers the surface plasmon resonance (SPR) of the energy acceptor, thereby transferring energy to the acceptor through a light radiation way. Both of these two forms of ET can effectively promote the recombination of the photogenerated electron–hole pairs of the energy donor. Therefore, the final result of the quenched photocurrent is the synergistic effect of the two paths in general. However, as displayed in Figure S1 in the SI, when R-CDs self-assembled to form R-CDs NS, their fluorescence disappeared, which means that the relaxation process through light radiation disappears, and the PRET process cannot happen. Therefore, the energy transfer process between R-CDs NS and AuNCs is mainly triggered by EET, which is the main cause for the quenched photocurrent of the system.

In order to explore the possible mechanism of the photocurrent enhancement on the TiO_2-modified electrode by the R-CDs NS, the band gap and energy band structure of R-CDs were characterized. First, the band gap of R-CDs NS was estimated by ultraviolet diffuse reflectance spectroscopy, as shown in Figure 3A, the optical band gap (E_g) of R-CDs NS was estimated to be 1.93 eV by the Tauc curve $(F(R)h\nu)^n = A(h\nu - E_g)$ and Kubelka–Munk (K–M) function.[31] As displayed in Figure 3B, the band edge of R-CDs NS is determined by ultraviolet photoelectron spectroscopy (UPS), and its energy levels of Fermi (E_F), valence band (E_{vb}), and conduction band (E_{cb}) are 3.87, 5.21, and 3.28 eV versus the vacuum level (E_{vac}), respectively. According to the conversion relationship between E_{vac} and RHE,[32] E_F, E_{vb}, and E_{cb} are −0.58, 0.76, and −1.17 V versus RHE, respectively, which match well with the energy band structure of n-type TiO_2.[12,33,34] The electron and energy transfer process before and after the FTO electrode was modified with TiO_2 and is shown in Figure 3C. When the FTO electrode was clean, the R-CDs NS was excited by the light source, and the photoelectrons transferred the energy to AuNCs in a non-radiative way and returned to the ground state and recombined with photogenerated holes, and fewer electrons flowed to the electrode surface, so the photocurrent decreased. When the FTO electrode was modified with TiO_2, TiO_2 on the electrode surface and the R-CDs NS in the solution were simultaneously excited by the light source, and the photogenerated electrons were rapidly transferred from the conduction band (C_B) of the R-CDs NS to the C_B of TiO_2 and flowed to the FTO electrode to generate photocurrent response. At the same time, the photogenerated holes were transferred from the valence band (V_B) of TiO_2 to the V_B of R-CDs NS, which effectively separated the photogenerated electrons and holes in time, inhibited the recombination of photogenerated electron–hole pairs, and made more electrons flow to the electrode, so the photocurrent of the system was significantly increased compared to the photocurrent obtained by clean FTO. Because the good photosensitized system consisted of TiO_2 and R-CDs was constructed, the impact of the ET process between AuNCs and R-CDs NS on the photocurrent of this photosensitized system was amplified, consequently, ET can result in a greater degree of signal change when FTO modified with TiO_2 and makes the sensor have a higher sensitivity.

Optimization of Experimental Conditions. To ensure the best sensing performance, several important experimental parameters were optimized. The concentration of HA is a key factor affecting the energy transfer between Au nanocages and R-CDs nanosheets. As displayed in Figure S2A in the SI, with the increase in HA concentration, the photocurrent of the control and experiment groups was increased gradually, and when the concentration of HA was 4.0 mg/mL, the Δphotocurrent (Δphotocurrent = $I - I_0$, where I_0 is the photocurrent in the absence of the target and I is the photocurrent in the presence of the 1.0 pM target) increased to its maximum; there may be two reasons: (i) the introduction of HA improved the hydrophilicity of R-CDs NS and boosted the limited charge transfer in solution caused by hydrophobicity of R-CDs NS, and (ii) when the concentration of HA increased, the thickness of the HA-modified layer gradually increased, which extended the distance and weakened the energy transfer effect between R-CDs nanosheets and AuNCs, which led to the increase in photocurrent. Δphotocurrent came to its maximum when the HA concentration was 4.0 mg/mL, so 4.0 mg/mL was the best concentration of HA.

https://doi.org/10.1021/acs.analchem.1c05081
Anal. Chem. 2022, 94, 1482–1490

The dosage of DSN was also important, and insufficient enzymes bring about low nicking efficiency, while superfluous enzymes may cause non-specific cleavage to generate a high background signal. Thus, the dosage of DSN was optimized, as illustrated in Figure S2B in the SI (black curve), and Δphotocurrent was enlarged with the augment of DSN and reached a platform until the dosage of DSN increased to 0.10 U; therefore, 0.10 U was the appropriate dosage of DSN. The enzymolysis time was another key factor; a short enzymolysis time may cause inadequate reaction, while a long enzymolysis time extends the detection time. Thus, the enzymolysis time from 10 to 60 min was investigated, as shown in Figure S2B in the SI (red curve), Δphotocurrent enlarged with the augment of time, and when the time was longer than 40 min, Δphotocurrent basically no longer increased, so 40 min was chosen for the DSN enzyme.

Analytical Performance of the ET-Based Sensing Platform. Under the optimal experimental conditions, the sensing performance of the biosensor was evaluated by the addition of the target with increasing concentrations. As shown in Figure 4A, when the target concentration increased from 0.2 fM to 1.0 nM (from a to j), the value of the photocurrent enlarged gradually. As illustrated in Figure 4B, a good linear relationship was obtained between the photocurrent intensity (I) and the logarithmic concentration of miRNA-155 (C_{target}) from 0.20 fM to 1.0 nM. The linear equation is as follows:

$$I\ (\mu A) = 0.249 \log C_{target}\ (pM) + 1.455\ (R^2 = 0.9948)$$

where R is the correlation coefficient and the limit of detection (LOD) was 71 aM (S/N = 3). As displayed in Table 1, when the proposed ET-based PEC sensor was compared with other miRNAs assays, this PEC sensor exhibited a lower LOD and wider linear range compared to previous studies.

Table 1. Comparison of the Developed PEC Biosensor with Other Strategies for miRNA Detection

method	linear range	LOD	references
fluorescence	1.0−500 fM	0.87 fM	35
electrochemistry	2.5 fM−25 nM	0.12 fM	36
electrochemiluminescence	1.0 fM−1.0 nM	0.5 fM	37
PEC	200 fM−25 nM	65 fM	4
PEC	0.5 fM−1.0 pM	0.18 fM	38
this work	0.20 fM−1.0 nM	71 aM	

Four possible interferents were utilized to investigate the selectivity of the ET-based PEC biosensor, the concentration of which was 1.0 pM, while the target concentration was 100 fM. As shown in Figure 5A, the single-base and three-base mismatched targets (SM-Target and TM-Target) lead to a negligible increase in photocurrent intensity. When miRNA-21 or miRNA-145 was used for sensing, the photocurrent intensity had no difference with the control group. When the 100 fM target containing 1.0 pM miRNA-21 and 1.0 pM miRNA-145 (mix) was used for PEC tests, the photocurrent intensity has no difference with the 100 fM target only, those results proved that the ET-based PEC sensing platform had good selectivity and high specificity for the target; whereafter, five independent biosensors were utilized for PEC tests in the presence of the 100 fM target to assess the reproducibility of the ET-based biosensor. The relative standard deviation (RSD) of the photocurrent intensities was 2.3%, indicating that the proposed ET-based sensing platform possessed good reproducibility.

Real Sample Analysis. To verify the analytical performance of the sensor in complex real samples, a recovery experiment in 10-fold diluted healthy human serum was carried out. As shown in Table 2, the recoveries were 99.6, 102.5, and 100.1%, respectively, and the RSD of three independent tests were 2.2−4.7%, which proved that the sensor had good analysis ability in a complex matrix. Moreover, MCF-7 (human breast cancer cell line) cell lysate was applied to evaluate the application potential of the ET-based biosensor. As shown in Figure 5B, when the cell number increased, the photocurrent intensity increased gradually because the miRNA-155 induced the disintegration of the nanocomposite and led to a photocurrent enhancement. It could be clearly observed that the photocurrent intensities of miRNA-155 extracted from MCF-7 were higher than that of the control group (black bar, cell number was 0). Those results proved that the ET-based PEC biosensor had good potential for detection miRNA-155 in actual samples.

Table 2. Recovery Experiment of the ET-Based Biosensor in 10-Fold Diluted Healthy Human Serum (n = 3)

samples	added	found	recovery (%)	RSD (%)
1	50.0 fM	49.80 fM	99.60	4.7
2	500 fM	512.3 pM	102.5	2.2
3	5.00 pM	5.040 pM	100.1	3.5

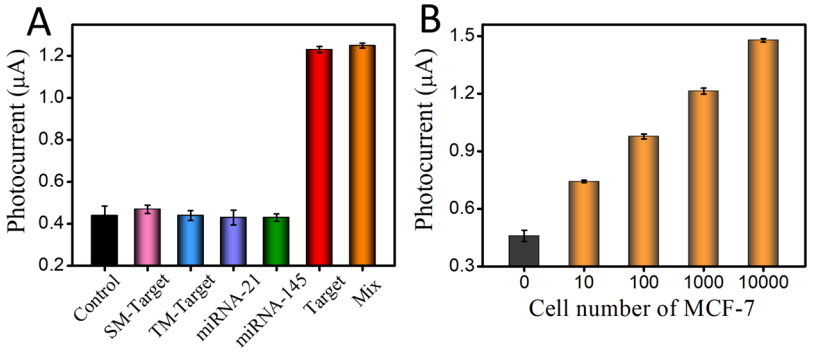

Figure 5. (A) Selectivity and (B) detection of miRNA-155 from MCF-7 cell lysate by the proposed PEC sensor. The error bars are standard deviation of three independent tests.

https://doi.org/10.1021/acs.analchem.1c05081
Anal. Chem. 2022, 94, 1482−1490

CONCLUSIONS

In summary, this research proposed a brand new ET system based on AuNCs and red emission carbon dot-assembled nanosheets (R-CDs NS). The system has been utilized to develop an ultrasensitive photoelectrochemical biosensor for microRNA detection. With TiO_2-modified FTO serving as the working electrode and the DSN enzyme-assisted target recycling strategy, the high sensitivity of the ET-based biosensor enable it to meet the real sample testing requirements. The ET-based PEC sensor also had high selectivity, good reproducibility, and stability and had the potential to detect miRNA in actual samples. By simply changing the sequence of ssDNA-1 and ssDNA-2, the sensing for various targets can be facilely realized.

ASSOCIATED CONTENT

Supporting Information

The Supporting Information is available free of charge at https://pubs.acs.org/doi/10.1021/acs.analchem.1c05081.

Additional experiment details (reagents and apparatus, cell culture and microRNAs extraction, oligonucleotide sequences information) and additional figures (fluorescence spectrum of R-CDs NS and optimization of experimental conditions) (PDF)

AUTHOR INFORMATION

Corresponding Authors

Jie Shen − *Department of Emergency and Critical Care Medicine, Jinshan Hospital, Fudan University, Shanghai 201508, China; Key Laboratory of Chemical Injury, Emergency and Critical Medicine of Shanghai Municipal Health Commission, Shanghai 201508, China;* Email: j1999sh@163.com

Lin Zhang − *Department of Emergency and Critical Care Medicine, Jinshan Hospital, Fudan University, Shanghai 201508, China; Key Laboratory of Chemical Injury, Emergency and Critical Medicine of Shanghai Municipal Health Commission, Shanghai 201508, China;* Email: linzhang0315@fudan.edu.cn

Zhenyu Lin − *Department of Emergency and Critical Care Medicine, Jinshan Hospital, Fudan University, Shanghai 201508, China; Ministry of Education Key Laboratory for Analytical Science of Food Safety and Biology, Fujian Provincial Key Laboratory of Analysis and Detection for Food Safety, College of Chemistry, Fuzhou University, Fuzhou, Fujian 350116, China; Key Laboratory of Chemical Injury, Emergency and Critical Medicine of Shanghai Municipal Health Commission, Shanghai 201508, China;* orcid.org/0000-0001-7890-6812; Phone: 86-0591-22866135; Email: zylin@fzu.edu.cn

Authors

Jiao Yang − *Department of Emergency and Critical Care Medicine, Jinshan Hospital, Fudan University, Shanghai 201508, China; Ministry of Education Key Laboratory for Analytical Science of Food Safety and Biology, Fujian Provincial Key Laboratory of Analysis and Detection for Food Safety, College of Chemistry, Fuzhou University, Fuzhou, Fujian 350116, China*

Fang Luo − *Ministry of Education Key Laboratory for Analytical Science of Food Safety and Biology, Fujian Provincial Key Laboratory of Analysis and Detection for Food Safety, College of Chemistry, Fuzhou University, Fuzhou, Fujian 350116, China;* orcid.org/0000-0003-1480-0677

Jian Wang − *Ministry of Education Key Laboratory for Analytical Science of Food Safety and Biology, Fujian Provincial Key Laboratory of Analysis and Detection for Food Safety, College of Chemistry, Fuzhou University, Fuzhou, Fujian 350116, China*

Bin Qiu − *Ministry of Education Key Laboratory for Analytical Science of Food Safety and Biology, Fujian Provincial Key Laboratory of Analysis and Detection for Food Safety, College of Chemistry, Fuzhou University, Fuzhou, Fujian 350116, China*

Complete contact information is available at: https://pubs.acs.org/10.1021/acs.analchem.1c05081

Notes

The authors declare no competing financial interest.

ACKNOWLEDGMENTS

The authors gratefully acknowledge the financial supports of the National Sciences Foundation of China (21974020, 81801943) and Research Grant for Public Health Key Discipline of Shanghai Municipality, China (No.GWV-10.1-XK26).

REFERENCES

(1) Hou, T.; Xu, N.; Wang, W.; Ge, L.; Li, F. *Anal. Chem.* **2018**, *90*, 9591−9597.
(2) Liu, X. P.; Chen, J. S.; Mao, C. J.; Niu, H. L.; Song, J. M.; Jin, B. K. *Biosens. Bioelectron.* **2018**, *116*, 23−29.
(3) Kim, K.; Lee, G. R.; Kim, M.; Lim, H.; Jung, Y. S.; Park, C. B. *ACS Nano* **2020**, *14*, 10376−10384.
(4) Song, X.; Hou, T.; Lu, F.; Wang, Y.; Liu, J.; Li, F. *Chem. Commun.* **2020**, *56*, 1811−1814.
(5) Yang, J.; Fu, S.; Luo, F.; Guo, L.; Qiu, B.; Lin, Z. *Microchim. Acta* **2021**, *188*, 267.
(6) Zhao, W. W.; Wang, J.; Xu, J. J.; Chen, H. Y. *Chem. Commun.* **2011**, *47*, 10990−10992.
(7) Zhao, W. W.; Yu, P. P.; Shan, Y.; Wang, J.; Xu, J. J.; Chen, H. Y. *Anal. Chem.* **2012**, *84*, 5892−5897.
(8) Dong, Y.-X.; Cao, J.-T.; Wang, B.; Ma, S.-H.; Liu, Y.-M. *ACS Sustainable Chem. Eng.* **2017**, *5*, 10840−10848.
(9) Shen, Q.; Han, L.; Fan, G.; Abdel-Halim, E. S.; Jiang, L.; Zhu, J. J. *Biosens. Bioelectron.* **2015**, *64*, 449−455.
(10) Chu, Y.; Han, T.; Deng, A.; Li, L.; Zhu, J.-J. *TrAC, Trends Anal. Chem.* **2020**, *123*, 115745.
(11) Wang, M.; Yin, H.; Zhou, Y.; Meng, X.; Waterhouse, G. I. N.; Ai, S. *Chem. Eng. J.* **2019**, *365*, 351−357.
(12) Gong, Y. T.; Yuan, F.; Dong, Y.; Li, Z.; Wang, G. L. *Anal. Chim. Acta* **2018**, *1014*, 19−26.
(13) Cheng, W.; Pan, J.; Yang, J.; Zheng, Z.; Lu, F.; Chen, Y.; Gao, W. *Microchim. Acta* **2018**, *185*, 263.
(14) Holá, K.; Sudolská, M.; Kalytchuk, S.; Nachtigallova, D.; Rogach, A. L.; Otyepka, M.; Zbořil, R. *ACS Nano* **2017**, *11*, 12402−12410.
(15) Lu, S.; Sui, L.; Liu, J.; Zhu, S.; Chen, A.; Jin, M.; Yang, B. *Adv. Mater.* **2017**, *29*, 1603443.
(16) Song, Y.; Zhu, C.; Song, J.; Li, H.; Du, D.; Lin, Y. *ACS Appl. Mater. Interfaces* **2017**, *9*, 7399−7405.
(17) Yang, H.; Liu, Y.; Guo, Z.; Lei, B.; Zhuang, J.; Zhang, X.; Liu, Z.; Hu, C. *Nat. Commun.* **2019**, *10*, 1789.
(18) Zhu, Z.; Zhai, Y.; Li, Z.; Zhu, P.; Mao, S.; Zhu, C.; Du, D.; Belfiore, L. A.; Tang, J.; Lin, Y. *Mater. Today* **2019**, *30*, 52−79.
(19) Shi, X.; Hu, Y.; Meng, H.-M.; Yang, J.; Qu, L.; Zhang, X.-B.; Li, Z. *Sens. Actuators, B* **2020**, *306*, 127582.

(20) Avvakumova, S.; Galbiati, E.; Sironi, L.; Locarno, S. A.; Gambini, L.; Macchi, C.; Pandolfi, L.; Ruscica, M.; Magni, P.; Collini, M.; Colombo, M.; Corsi, F.; Chirico, G.; Romeo, S.; Prosperi, D. *Bioconjugate Chem.* **2016**, *27*, 2911−2922.
(21) Chen, J.; Yang, M.; Zhang, Q.; Cho, E. C.; Cobley, C. M.; Kim, C.; Glaus, C.; Wang, L. V.; Welch, M. J.; Xia, Y. *Adv. Funct. Mater.* **2010**, *20*, 3684−3694.
(22) Cheng, H.; Huo, D.; Zhu, C.; Shen, S.; Wang, W.; Li, H.; Zhu, Z.; Xia, Y. *Biomaterials* **2018**, *178*, 517−526.
(23) Wan, J.; Geng, S.; Zhao, H.; Peng, X.; Xu, J.; Wei, M.; Mao, J.; Zhou, Y.; Zhu, Q.; Zhao, Y.; Yang, X. *Nanoscale* **2018**, *10*, 20020−20032.
(24) Xia, Y.; Li, W.; Cobley, C. M.; Chen, J.; Xia, X.; Zhang, Q.; Yang, M.; Cho, E. C.; Brown, P. K. *Acc. Chem. Res.* **2011**, *44*, 914−924.
(25) Skrabalak, S. E.; Au, L.; Li, X.; Xia, Y. *Nat. Protoc.* **2007**, *2*, 2182−2190.
(26) He, Y.; Yang, X.; Yuan, R.; Chai, Y. *Anal. Chem.* **2017**, *89*, 2866−2872.
(27) Wu, Y.; He, Y.; Yang, X.; Yuan, R.; Chai, Y. *Sens. Actuators, B* **2018**, *275*, 260−266.
(28) Yang, X.; Wang, S.; Wang, Y.; He, Y.; Chai, Y.; Yuan, R. *ACS Appl. Mater. Interfaces* **2018**, *10*, 12491−12496.
(29) Zhang, Q.; Li, W.; Wen, L. P.; Chen, J.; Xia, Y. *Chemistry* **2010**, *16*, 10234−10239.
(30) Ma, Z. Y.; Ruan, Y. F.; Xu, F.; Zhao, W. W.; Xu, J. J.; Chen, H. Y. *Anal. Chem.* **2016**, *88*, 3864−3871.
(31) Pathak, A.; Shen, J. W.; Usman, M.; Wei, L. F.; Mendiratta, S.; Chang, Y. S.; Sainbileg, B.; Ngue, C. M.; Chen, R. S.; Hayashi, M.; Luo, T. T.; Chen, F. R.; Chen, K. H.; Tseng, T. W.; Chen, L. C.; Lu, K. L. *Nat. Commun.* **2019**, *10*, 1721.
(32) Yang, Y.; Wang, S.; Jiao, Y.; Wang, Z.; Xiao, M.; Du, A.; Li, Y.; Wang, J.; Wang, L. *Adv. Funct. Mater.* **2018**, *28*, 1805698.
(33) Zhao, W.-W.; Shan, S.; Ma, Z.-Y.; Wan, L.-N.; Xu, J.-J.; Chen, H.-Y. *Anal. Chem.* **2013**, *85*, 11686−11690.
(34) Cakiroglu, B.; Ozacar, M. *Biosens. Bioelectron.* **2018**, *119*, 34−41.
(35) Wu, H.; Wu, J.; Liu, Y.; Wang, H.; Zou, P. *Microchim. Acta* **2019**, *186*, 715.
(36) Guo, W. J.; Wu, Z.; Yang, X. Y.; Pang, D. W.; Zhang, Z. L. *Biosens. Bioelectron.* **2019**, *131*, 267−273.
(37) Feng, Q.-M.; Shen, Y.-Z.; Li, M.-X.; Zhang, Z.-L.; Zhao, W.; Xu, J.-J.; Chen, H.-Y. *Anal. Chem.* **2016**, *88*, 937−944.
(38) Wang, M.; Yin, H.; Zhou, Y.; Han, J.; He, T.; Cui, L.; Ai, S. *Microchim. Acta* **2018**, *185*, 257.

https://doi.org/10.1021/acs.analchem.1c05081
Anal. Chem. 2022, 94, 1482−1490